BMC Cancer

RESEARCH Open Access

Synthetic lethality from the combination of a histone methyltransferase SUV39H2 inhibitor and a poly (ADP-ribose) polymerase inhibitor for uterine leiomyosarcoma

Yusuke Toyohara[1,2], Kenbun Sone[1*], Kohei Kumegawa[3], Yoko Yamamoto[1], Ryuta Hachijo[1,2], Asako Kukita[1], Ayumi Taguchi[1], Masako Ikemura[4], Yuichiro Miyamoto[1], Michihiro Tanikawa[1], Takayuki Iriyama[1], Mayuyo Mori[1], Ryuji Hamamoto[5,6], Tetsuo Ushiku[4], Katsuhiko Oda[7], Yasushi Hirota[1], Reo Maruyama[2,3] and Yutaka Osuga[1]

Abstract

Background Uterine leiomyosarcoma (uLMS) has a poor prognosis owing to its resistance to chemotherapy. Therefore, novel therapeutic targets for uLMS should be identified.

Suppressor license of variegation 3–9 homolog 2 (SUV39H2) is a histone methyltransferase that promotes the repair of double-strand DNA breaks by recruiting phosphorylated H2AX (γH2AX). In this study, we investigated the potential therapeutic targets of SUV39H2 in uLMS and the mechanism of synthetic lethality between PARP inhibitors and the SUV39H2 inhibitor OTS186935.

Methods First, we analyzed the mRNA and protein expression of *SUV39H2* in the clinical tissues of uLMS, normal myometrium, and leiomyomas using real-time polymerase chain reaction and immunohistochemistry, respectively. Next, we conducted drug sensitivity assays for OTS186935 alone and in combination with olaparib, a poly (ADP-ribose) polymerase inhibitor, using the uLMS cell lines SK-LMS-1 and SK-UT-1. We performed western blotting, immunofluorescence, and chromatin immunoprecipitation sequencing (ChIP-seq) to investigate γH2AX following OTS186935 treatment in addition to in vivo experiments using nude mice with subcutaneously implanted uLMS.

Results *SUV39H2* expression in uLMS was significantly higher than that in the normal myometrium and leiomyomas. OTS186935 decreased the viability of both cell lines, and its combination with olaparib resulted in synthetic lethality in SK-UT-1 cells (combination index = 0.88). After treatment with OTS186935, γH2AX accumulation decreased. ChIP-seq also showed downregulation of γH2AX following OTS186935 treatment. Notably, the combination of OTS186935 and a PARP inhibitor was significantly more effective in vivo.

Conclusion OTS186935 inhibited double-strand DNA break repair, as evidenced by γH2AX downregulation by ChIP-seq and other assays. Combining OTS186935 with olaparib demonstrated activity resembling synthetic lethality; however, further validation is required before clinical translation.

*Correspondence:
Kenbun Sone
ksone5274@gmail.com

Full list of author information is available at the end of the article

Keywords SUV39H2, Uterine leiomyosarcoma, γH2AX, PARP inhibitor, Synthetic lethality

Background

Uterine leiomyosarcoma (uLMS) is a soft tissue sarcoma that arises from the mesenchymal tissue of the uterus [1]. uLMS is a major subtype of uterine sarcoma and accounts for 63% of all uterine sarcoma cases. Primary total hysterectomy and bilateral salpingo-oophorectomy are recommended to treat uLMS [1]. Although advanced uLMS is generally treated with doxorubicin-based chemotherapy [2], it has a high recurrence rate that ranges from 53 to 71%, resulting in poor prognosis [3]. While some molecular targeted therapies have been approved for uLMS, the response rates remain low and have not significantly improved prognosis [4–6]. Recently, poly (ADP-ribose) polymerase (PARP) inhibitors for uLMS have been introduced, and phase II clinical trials have begun [7, 8] because 25% of patients with uLMS had homologous recombination repair defects (HRD) [9]. PARP inhibitors can be used in patients with HRD because cells with HRD rely on alternative repair mechanisms, including non-homologous end joining (NHEJ) and single-strand break repair, which play a role in PARP [10]. However, the acquisition of resistance to PARP inhibitors has become a concern.

In cancer research, epigenetic studies have focused on elucidating carcinogenesis, cancer metastasis, and novel therapeutic strategies. Epigenetics reversibly regulates gene expression without altering the DNA sequence. Chromatin remodeling regulates gene expression and is involved in the transcriptional activity and repression of each gene. Epigenetics comprises three main components: DNA methylation, histone modification, and non-coding RNA-associated gene silencing [11]. The aberrant regulation of histone modification is believed to contribute to cancer development [11, 12].

In 2020, the Food and Drug Administration approved tazemetostat, a histone methyltransferase EZH2 inhibitor, for treatment-resistant epithelioid sarcoma and follicular lymphoma with EZH2 mutations [13]. Therefore, the clinical application of histone methyltransferase inhibitors has attracted attention as a novel therapeutic strategy for cancer. Our group previously investigated histone methyltransferases and demonstrated their efficacy in gynecological cancers [14–17]. Using EZH2 and PARP inhibitors, Karakashev et al. reported that CARM1 induces a synthetic lethal mechanism in high-grade serous ovarian cancers that highly express CARM1 [18]. Histone methyltransferase combined with PARP inhibitors enhanced the efficacy of PARP inhibitors and may provide insights into overcoming PARP inhibitor resistance.

Suppressor license of variegation 3–9 homolog 2 (SUV39H2), a histone methyltransferase, is responsible for regulating gene expression by catalyzing the trimethylation of histone H3 lysine 9 (H3K9me3). When DNA damage occurs, phosphorylated H2AX (γH2AX) is induced, which activates double-strand DNA break repair mechanisms. SUV39H2 is reportedly involved in γH2AX recruitment, and its suppression reduces γH2AX activity [19]. Additionally, SUV39H1/2 is required for homologous recombination repair (HRR), and when SUV39H1/2 is defective, cells appear to have HRD-like status [20]. Because of its high expression in multiple cancers [21–23] and involvement in DNA break repair mechanisms, SUV39H2 has been used as a novel therapeutic target. Specific inhibitors of SUV39H2 have been developed (OTS186935) [23], which regulate the production of γH2AX and have shown efficacy in in vitro and in vivo experiments on breast cancer.

This study aimed to evaluate the efficacy of an SUV39H2 inhibitor alone and in combination with a PARP inhibitor against uLMS, to develop a novel therapeutic approach based on an epigenetics-based target.

Methods

Clinical tissue samples and ethical statement

Clinical tissue specimens for gene expression analysis and immunohistochemical staining (IHC) were obtained during gynecological surgeries performed at the University of Tokyo Hospital. For gene expression analysis, specimens were collected in 5–10 mm squares, flash-frozen, and stored in a −80 °C freezer. Additionally, 4 μm thick slices of formalin-fixed paraffin-embedded specimens were used for IHC.

Cell lines

SK-LMS-1 (ATCC, Manassas, VA, USA; Cat. # HTB-88) and SK-UT-1 (Cat. # HTB-114) were used as uLMS cell lines and were cultivated in Eagle's minimum essential medium (E-MEM, FUJIFILM Wako Pure Chemical Corporation, Osaka, Japan) supplemented with 10% heat-inactivated fetal bovine serum (Thermo Fisher Scientific, MA, USA) and 1% penicillin/streptomycin (FUJIFILM Wako Pure Chemical Corporation). The cells were maintained in an incubator at 37 °C with 5% CO_2. The cell lines were subjected to FASMAC Short Tandem Repeat analysis for cell authentication.

Total RNA extraction and mRNA expression analysis of clinical tissue specimens and cell lines

Clinical specimens and RLT buffer with 1% 2-mercaptoethanol (FUJIFILM Wako Pure Chemical Corporation)

were mixed in MagNA Lyser Green Beads (Roche Diagnostics, Indianapolis, IN, USA) using a MagNA Lyser (Roche, Basel, Switzerland) (6,500 rpm for 70 s). The homogenates were subsequently centrifuged (14,000 rpm for 3 min). The supernatant was collected, and total RNA was extracted using the RNeasy Mini Kit (Qiagen, Hilden, Germany) following the manufacturer's instructions. Complementary DNA was synthesized by reverse transcription using ReverTra Ace (Toyobo, Osaka, Japan).

Real-time quantitative polymerase chain reaction (RT-qPCR) was performed on a QuantStudio 1 Real-Time PCR System (Thermo Fisher Scientific) using KOD SYBR qPCR Mix (Toyobo). The mRNA expression levels in the tissue samples and cell lines were confirmed and normalized using the $2^{-\Delta\Delta CT}$ method. *ACTB* was used as an internal control. Table S1 (Additional file 1) shows the primer sequences.

IHC

After deparaffinization and antigen activation by heating (95 °C, 20 min), an anti-SUV39H2 antibody (Abcam, Cambridge, UK; Cat. # ab190870; 1:200) was added to the slides and incubated overnight at 4 °C. Nuclear staining was performed using hematoxylin. Each specimen was evaluated using the IHC score, which is the sum of the proportion score (PS) and intensity score (IS). PS was calculated as the proportion of positive cells as follows: 0 = 0%; 1 = < 1%; 2 = 1–10%; 3 = 10–33%; 4 = 33–67%; and 5 = > 67%. IS was graded as 0 (negative), 1 (weak), 2 (intermediate), and 3 (strong). Two technicians independently evaluated the IHC scores, and the mean was calculated for each IHC score.

Drug sensitivity assay

Tazemetostat/EPZ-6438 (MedChemExpress, NJ, USA), an EZH2 inhibitor; OTS186935 (MedChemExpress), an SUV39H2 inhibitor; and olaparib (MedChemExpress), a PARP inhibitor, were used in this study. Each inhibitor was dissolved in 0.1% dimethylsulfoxide (DMSO; Sigma–Aldrich). For the drug sensitivity assay, SK-LMS-1 and SK-UT-1 cells were pre-cultured. After 72 h or 96 h of incubation with a new medium diluted to the target concentration of the inhibitors, cell viability was evaluated using a cell counting kit-8 (DOJINDO, Kumamoto, Japan), while absorbance was measured with a microplate reader (BioTek, VT, USA). Three independent experiments were performed. Wells incubated with 0.1% DMSO were used as controls, and the ratio of absorbance at the desired concentration was calculated, with the absorbance of the control as 100%.

A combination index (CI) was used [24]. The CI, which was the half-maximal inhibitory concentration (IC_{50}) of the two drugs combined versus the IC_{50} of a single drug, was calculated as follows:

$$CI = \frac{D1}{Dx} + \frac{D2}{Dx} \times 2$$

where (D1) and (D2) are the IC_{50} of drugs 1 and 2, respectively, when combined, and.

(Dx) 1 and (Dx) 2 are the respective IC_{50} of drugs 1 and 2 as single agents. The obtained CIs were classified as synergistic (CI < 1), additive (CI = 1), and antagonistic (CI > 1).

Colony formation assay

Six-well plates were pre-cultured with SK-LMS-1 and SK-UT-1 cells. After cell attachment, the medium was replaced with fresh medium containing the inhibitor at the target concentration, prepared by diluting the stock solution in culture medium (final DMSO 0.1%). The medium was replaced every 3 days, and the cells were fixed and stained on days 10–12. The number of colonies (> 50 cells) was counted under a microscope. Three wells were analyzed for each concentration.

Western blotting

For protein extraction, the cell pellet was suspended in sodium dodecyl sulfate (SDS) lysis buffer (0.1 M Tris–HCl, pH 7.5, 10% glycerol [FUJIFILM Wako], and 2% SDS [FUJIFILM Wako Pure Chemical Corporation]). The supernatant was collected through centrifugation (15,000 rpm, 10 min, 4 °C) after heating at 95 °C for 5 min. Mini-PROTEAN TGX Precast Protein Gels (Bio-Rad, Hercules, CA, USA) were used for SDS polyacrylamide gel electrophoresis. The separated samples were transferred via a semi-dry transfer method using Trans-Blot Turbo Mini PVDF Transfer Packs (Bio-Rad). Amersham ECL Select (Cytiva, MA, USA) or SuperSignal™ West Femto (Thermo Fisher Scientific) were used as chemiluminescent reagents, and detection was performed using ImageQuant LAS 4000 (GE Healthcare Life Sciences, NJ, USA).

The antibodies used are listed in Table S2 (Additional file 1). All primary reactions were performed overnight at 4 °C.

Cell cycle analysis and annexin assay

For cell cycle analysis, cells were fixed using 70% ethanol after incubation with the target concentrations of the inhibitors, followed by nucleic acid staining with propidium iodide (Sigma–Aldrich).

For the annexin assay, the fluorescence intensity of the cells was determined using a BD FACSCalibur HG Flow Cytometer (BD Biosciences, Franklin Lakes, NJ, USA). Cell cycle and annexin assays were analyzed using FlowJo software version 16 (FlowJo LLC, OR, USA). For the annexin assay, the percentages of early and late apoptotic cell populations were summed to calculate the

percentage of apoptotic cells. Three independent experiments were performed.

Cell immunofluorescence staining

Doxorubicin (DOX; Cayman Chemical Company) was used to induce DNA damage. uLMS cell lines were incubated on microcover glass (Matsunami Glass Ind., Ltd., Osaka, Japan) on 35-mm plates with the target concentrations of inhibitors until the targeted time, and fixation was performed using 4% paraformaldehyde phosphate buffer solution (FUJIFILM Wako Pure Chemical Corporation). After permeabilization with 0.05% Tween-20 (Sigma–Aldrich) for 5 min twice and 0.5% TritonX-100 (Sigma–Aldrich) for 10 min, the cells were incubated in 3% bovine serum albumin (BSA, FUJIFILM Wako Pure Chemical Corporation) for 60 min at 25 °C. Primary antibodies (see Additional file 1: Table S2) were diluted in 3% BSA and incubated overnight at 4 °C in a wet box. After permeabilization, the cells were incubated with a secondary antibody (see Additional file 1: Table S2) and 4',6-diamidino-2-phenylindole for nuclear staining for 60 min at 25 °C. After washing the cells on the glass, the cover glass was encapsulated and observed under a confocal fluorescence microscope (LSM880; Carl Zeiss Co., Ltd., Oberkochen, Germany). Imaging was performed using ImageJ 1.53. Subsequently, the relative intensity of γH2AX in each cell was estimated.

RNA sequencing (RNA-seq)

Total RNA was extracted using the abovementioned method and techniciansutilized for library preparation through the SMARTer Stranded Total RNA Sample Prep Kit (TaKaRa Bio, Tokyo, Japan). Libraries were sequenced using NextSeq 550 (Illumina, San Diego, CA, USA) with paired-end reads.

Chromatin immunoprecipitation (ChIP) sequencing

After culturing, 5×10^6 uLMS cells were collected using 0.25% trypsin–EDTA (FUJIFILM Wako Pure Chemical Corporation). The cell pellets were cross-linked with 1% formaldehyde solution (FUJIFILM Wako Pure Chemical Corporation) for 10 min at 37 °C and treated with 0.125 M glycine (FUJIFILM Wako Pure Chemical Corporation) for 5 min at 25 °C. After lysing the cells in lysis buffer (see Additional file 1: Table S3), DNA fragmentation was performed by sonication with a Covaris S220 (Covaris, Woburn, MA, USA) for 200 cycles for 10 min. The fragmented DNA underwent ChIP and was incubated overnight at 4 °C with Dynabeads Protein G (Thermo Fisher Scientific) and 2.5 μg of anti-gamma H2A.X (phospho S139) antibody (Abcam, Cat. #ab2893, Lot: GR3446449-2). Next, we washed the beads with low-salt, high-salt, and LiCl immune complex wash buffers (see Additional file 1: Table S3) at 4 °C for 5 min, followed by washing with TE buffer (see Additional file 1: Table S3) for 5 min at 25 °C. The fragments were extracted using an elution buffer (see Additional file 1: Table S3). Libraries were prepared using a ThruPLEX DNA-Seq Kit (TaKaRa Bio). Sequencing was performed with paired-end reads using NextSeq 550, following the same method employed for RNA-seq.

Sequencing data analysis

For RNA-seq analysis, sequence reads were trimmed to extract adaptor sequences using Skewer (v0.2.2) [25] and mapped to the hg38 genome using spliced transcript alignment to a reference (v.2.7.8a) [26]. Mapped reads were counted using feature counts (v.2.0.10) [27]. Integrative Genomic Viewer (v2.11.1) [28] was used to visualize the mapped reads. In chromatin immunoprecipitation sequencing (ChIP-seq) analysis, raw reads were aligned to hg38 using bowtie2 (v.2.4.2) [29]. Multialigned reads and PCR copies were eliminated using Picard (v.2.25.3; http://broadinstitute.github.io/picard/). Bedtools (v2.30.0) [30] was utilized to filter reads that overlapped with the blacklist of the Encyclopedia of DNA Elements (ENCODE). MACS2 (v 2.2.7.1) [31] was used to call peaks with the parameter "–keep-dup auto -q 0.1." Ngsplot was utilized to visualize peak signals within a range of ± 1,000 bp around the γH2AX peaks in doxorubicin-treated cells [32].

In vivo *experiments*

Animal experiments were performed following the ARRIVE guidelines 2.0 and were approved by the Animal Experiment Committee of the Graduate School of Medicine, University of Tokyo (Approval No.-H20-243). We used 5-week-old immunodeficient BALB/cAJcl-nu/nu mice purchased from CLEA Japan, Inc. Mice were maintained on a 12-h day/night cycle and kept in a clean environment with adequate food and water. SK-UT-1 cells were suspended at 5×10^6 cells in a total volume of 150 μL comprising 50 μL Matrigel (Corning, NY, USA) and 100 μL E-MEM, and injected subcutaneously into the dorsal subcutaneous tissue of nude mice under inhalation anesthesia sedation. Tumor volume was calculated using the following formula: tumor volume = (tumor short diameter)^2 × (tumor long diameter)/2. Treatment was initiated when the tumor diameter reached 5 mm. Drugs were administered intraperitoneally under the following conditions: DMSO for the control group, 10 mg/kg OTS186935 for the OTS186935 group, 50 mg/kg olaparib for the olaparib group, and a combination of 10 mg/kg OTS186935 with 50 mg/kg olaparib for the combination group. Each group comprised six mice. All drugs were dissolved in 10% DMSO and PEG300 in 200 μL of saline. Tumor size was measured every 2–3 days and evaluated on day 14 after treatment initiation. At the end of the

experiment, mice were euthanized under deep anesthesia with isoflurane (inhalation), in accordance with institutional guidelines and approved protocols.

Statistical analysis

Each experiment was independently performed at least three times, and the data were calculated as the mean ± standard deviation. Student's *t*-test was used to analyze the data. Due to the limited number of clinical samples, the mRNA expression and IHC analyses, initially designed to involve three groups, were instead evaluated as two-group comparisons—uLMS vs. normal uterine myometrium and uLMS vs. uterine leiomyomas. In vivo studies included four treatment arms; statistical testing was performed as pairwise two-group comparisons between prespecified pairs (e.g., control vs. OTS186935, control vs. olaparib, OTS186935 vs. olaparib, and combination vs. each monotherapy). Differences were considered statistically significant at $P < 0.05$. A one-sided test was used for mRNA expression analysis of clinical samples, and a two-sided test was employed for other samples. All statistical analyses were performed using Microsoft Excel and R (version 4.3.1; R Foundation for Statistical Computing, Vienna, Austria).

Results

Expression analysis in clinical tissue samples and drug sensitivity assays

mRNA expression levels of 11 histone methyltransferases were quantified using RT-qPCR in clinical tissue samples from normal uterine myometrium ($n = 4$), uterine leiomyomas ($n = 4$), and uLMS ($n = 6$) (see Additional File 1: Table S4). Significant upregulation of *EZH2*, *SUV39H2*, and *WHSC1* was observed in uLMS compared to both normal uterine myometrium and uterine leiomyomas (Fig. 1A, B).

Among these three histone methyltransferases, selective inhibitors are available for *SUV39H2* and *EZH2*. The efficacy of OTS186935 and EPZ-6438 was evaluated in the uLMS cell lines SK-LMS-1 and SK-UT-1. EPZ-6438 showed no efficacy against either cell line (see Additional File 2: Fig. S1A), while OTS186935 demonstrated dose-dependent cytotoxicity, with IC_{50} values of 1.16 μM and 1.04 μM for SK-LMS-1 and SK-UT-1, respectively (Fig. 1C).

SUV39H2 protein expression in clinical specimens was further assessed through IHC (see Additional File 1: Table S5). As shown in Fig. 1D, staining intensity was categorized as negative, weak, intermediate, or strong. uLMS tissues exhibited significantly higher IHC scores than normal myometrium and uterine leiomyomas (Fig. 1E and Additional File 3: Fig. S1B).

Combination therapy with OTS186935 and olaparib

To elucidate the mechanism of action of OTS186935, we performed western blotting to assess ttechnicianshe levels of H3K9me3, a histone modification catalyzed by SUV39H2. The results demonstrated that OTS186935 reduced H3K9me3 levels (Fig. 2A and Additional File 8: Fig. S6A), indicating inhibition of SUV39H2. We next examined the combinatorial effects of OTS186935 and olaparib in uLMS cell lines. As determined by the cell viability assay, the CI was 0.97 (95% confidence interval, 0.95–0.98) for SK-LMS-1. The IC_{50} values were 11.1 μM (9.3–12.8) for olaparib and 1.04 μM (1.03–1.06) for OTS186935 when tested individually, while in combination, the values were 1 μM and 0.91 μM (0.89–0.94), respectively. In SK-UT-1 cells, the CI was 0.88 (0.83–0.93); the IC_{50} values of were 7.03 μM (6.72–7.70) for olaparib and 1.66 μM (1.59–1.71) for OTS186935, while in combination, the values were 2.5 μM and 0.88 μM (0.83–0.92), respectively (Fig. 2B and Additional File 4: Fig. S2). According to Chou et al., a $CI < 0.9$ indicates a synergistic effect [24]. Therefore, the CI for SK-UT-1 demonstrated synergism. To evaluate the long-term efficacy of the combination treatment, a colony formation assay was conducted (Fig. 2C), which further confirmed the synergistic effect in SK-UT-1 compared to SK-LMS-1.

Elucidation of the synergistic effect in SK-UT-1

We investigated the mechanisms underlying the synergistic effect in SK-UT-1 compared to that in SK-LMS-1 and the cell cycle analysis results. After treatment with OTS186935 alone, the G2/M phase was significantly increased in both SK-LMS-1 and SK-UT-1. However, when olaparib was added, no significant change was observed in the cell cycle of either cell line (Fig. 3A).

Next, we evaluated the induction of apoptosis using an annexin assay. No significant increase was observed in the percentage of apoptotic cells in SK-LMS-1 following combination therapy (see Additional file 5: Fig. S3). In contrast, a significant increase was detected in apoptotic cells in SK-UT-1 when OTS186935 was combined with olaparib (Fig. 3B).

Similar to the results of the annexin assay, apoptosis was observed in SK-UT-1 cells after combination treatment in the detection of cleaved PARP, which was not observed in SK-LMS-1 cells (Fig. 3C and Additional File 8: Fig. S6B).

We hypothesized that the synergistic effects of OTS186935 and olaparib on SK-UT-1 cells may be related to factors involved in DNA damage/repair mechanisms. We investigated the DepMap Portal (https://depmap.org/portal/, accessed on 3/2/2022) and found a deletion in 53BP1 in SK-UT-1 cells. Deletion of 53BP1 in SK-UT-1 cells caused a frameshift mutation, whereas deletion in SK-LMS-1 cells did not result in abnormalities.

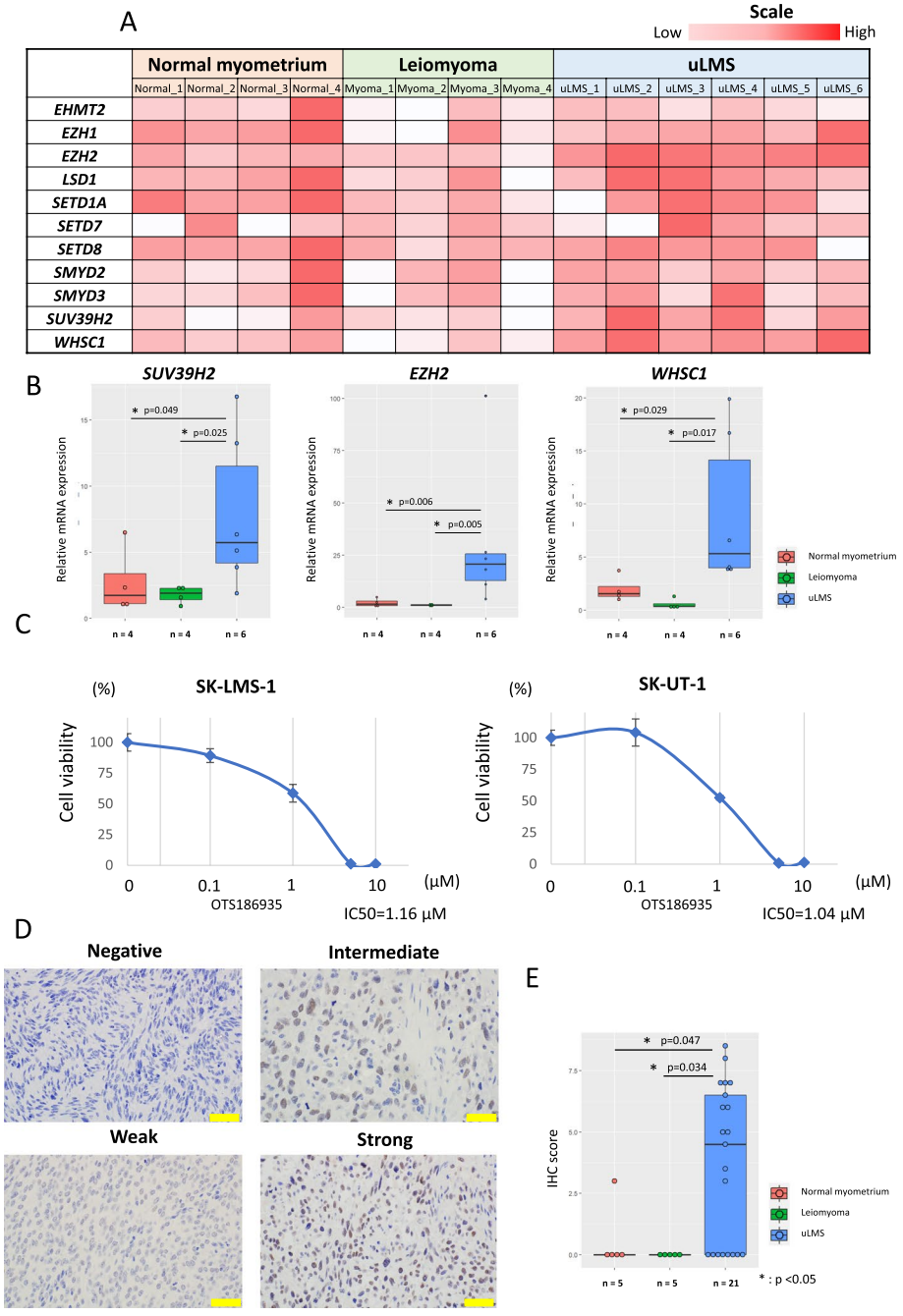

Fig. 1 Expression analysis in clinical tissue samples and drug sensitivity assays. **A** RT-qPCR of 11 types of histone methyltransferases in uLMS, normal uterine myometrium, and uterine leiomyomas. mRNA expression levels were normalized using the $2^{-\Delta\Delta CT}$ method, and the relative expression is shown. Red represents high expression in the heatmap. **B** Expression levels of the three genes overexpressed in uLMS (*SUV39H2*, *EZH2*, and *WHSC1*) were compared in two-group analyses of uLMS vs. normal uterine myometrium and uLMS vs. uterine leiomyomas. *P* values for each gene are shown. Significant differences were assessed using a prespecified one-sided Student's t-test (uLMS > comparator). Asterisks indicate $p < 0.05$. Bars = mean ± SD; n = cases (biological replicates). **C** Drug sensitivity assay for OTS186935. SK-LMS-1 and SK-UT-1 after treatment with OTS186935 (0.1–10 μM) for 96 h. Bars = mean ± SD. **D** IHC for SUV39H2 in clinical samples. Representative images of the intensity score, which was defined as score 0 = negative; 1 = weak; 2 = intermediate; and 3 = strong. The yellow bar indicates 50 μm. **E** IHC scores of SUV39H2 in uLMS, normal uterine myometrium, and uterine leiomyomas. Two-group comparisons were performed for uLMS vs. normal uterine myometrium and uLMS vs. uterine leiomyomas. Significant differences were assessed using two-sided Student's t-tests (p values shown). Asterisks indicate $p < 0.05$. Bars = mean ± SD; *n* = cases (biological replicates). RT-qPCR, real-time quantitative polymerase chain reaction; IHC, immunohistochemical staining; SD, standard deviation; uLMS, uterine leiomyosarcoma

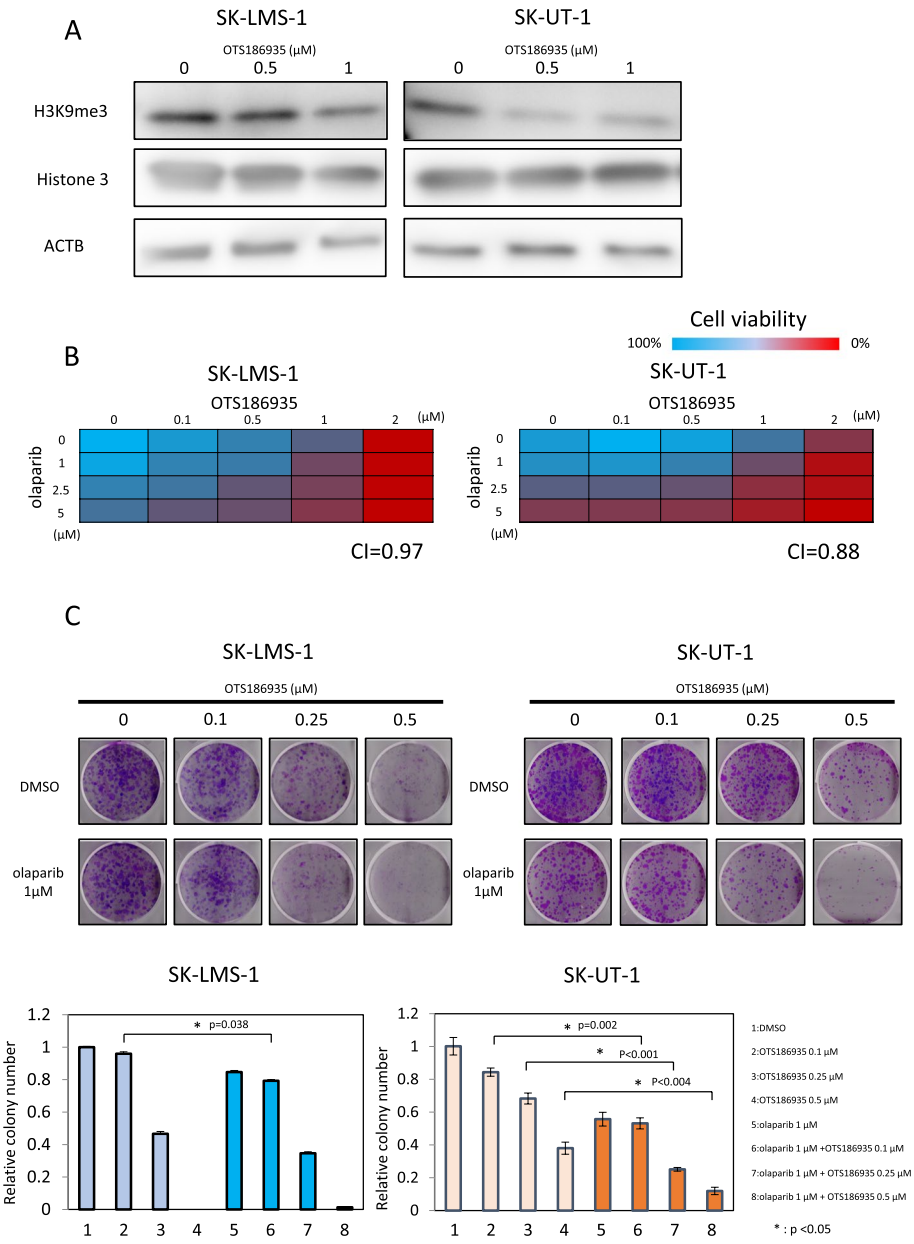

Fig. 2 Effect of OTS186935 combined with olaparib. **A** Inhibition of SUV39H2 decreased H3K9me3 expression in both SK-LMS-1 and SK-UT-1 cell lines after treatment with 0.5–1 μM of OTS186935 or 0.1% of DMSO for 48 h. **B** Cell viability assay for OTS186935 combined with olaparib. Cell viability was expressed as a heatmap. The CI of SK-UT-1 and SK-LMS-1 was 0.97 (95% confidence interval, 0.95–0.98) and 0.88 (95% confidence interval, 0.83–0.93), respectively. **C** Colony formation assay for the combination of OTS186935 and olaparib. Cell lines were treated with 0.1–0.5 μM of OTS186935, 1 μM of olaparib, or 0.1% of DMSO for 12 days. Significant differences were analyzed using the two-sided Student's t-test. Asterisks indicate *p*-values < 0.05. Bars = mean ± SD; *n* = 3 independent experiments (per condition). CI, combination index; SD, standard deviation; DMSO, dimethylsulfoxide

We conducted RNA-seq of SK-UT-1 cells, revealing p.T1060PfsTer36 of *TP53BP1* (see Additional file 6: Fig. S4A). We also conducted immunofluorescence staining on both cell lines, and TP53BP1 expression was relatively weak in SK-UT-1 compared to that in SK-LMS-1 (see Additional file 6: Fig. S4B).

Mechanism of OTS186935 on the DNA break repair pathway

Next, we investigated the effects of OTS186935 on DNA repair after doxorubicin-induced DNA breaks. We added 0.1% DMSO for the negative control, 1 μM of OTS186935, 0.5 μM of doxorubicin, and OTS186935 1 μM + doxorubicin 0.5 μM to each of the uLMS cell lines. Doxorubicin treatment resulted in γH2AX accumulation, whereas the combination with OTS186935

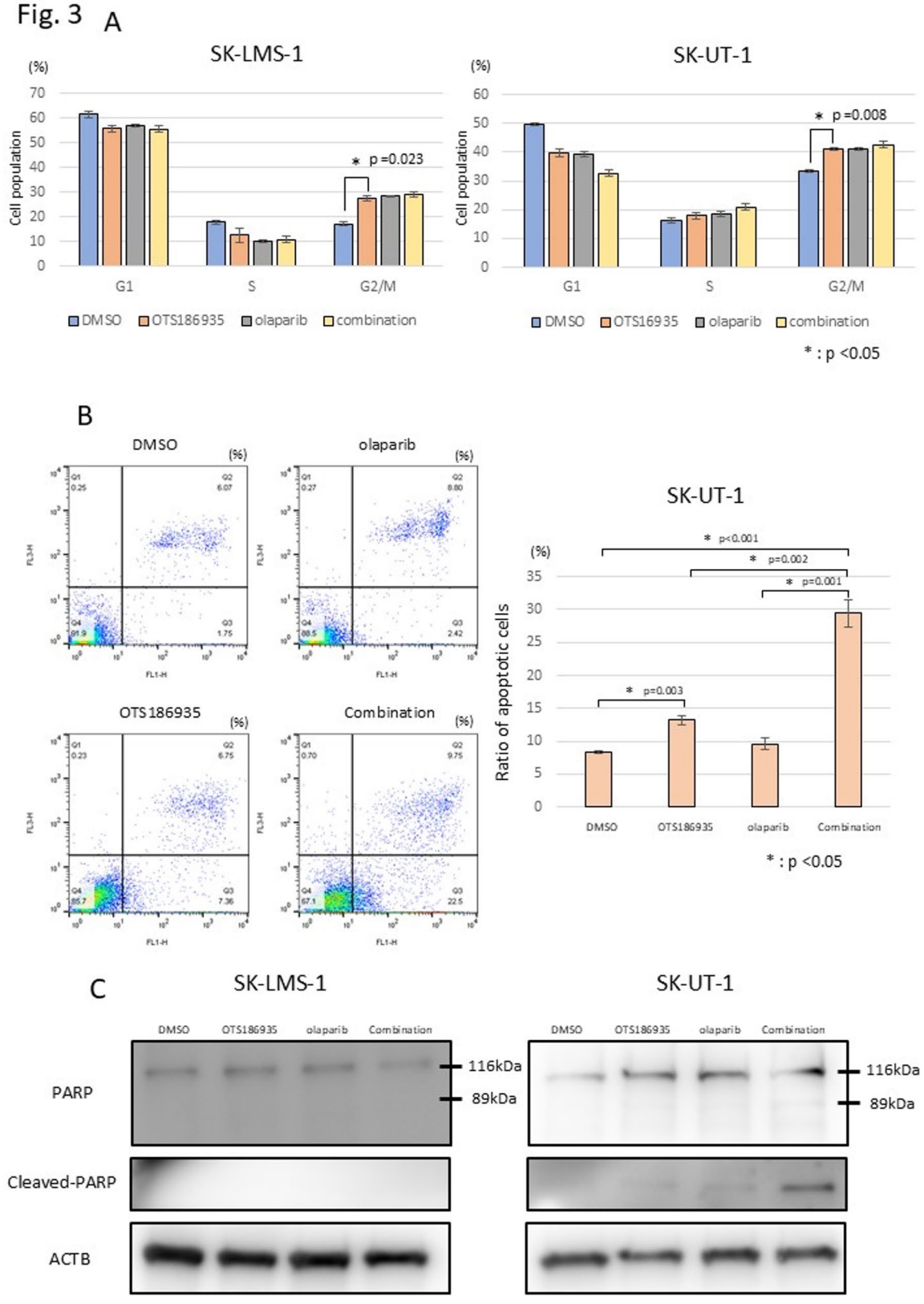

Fig. 3 (See legend on next page.)

(See figure on previous page.)

Fig. 3 Elucidation of the mechanism of the synergistic effect in SK-UT-1. **A** Cell cycle assay of SK-LMS-1 and SK-UT-1 after treatment with 0.1% DMSO, 0.5 μM OTS186935, 1 μM olaparib, and 0.5 μM OTS186935 + 1 μM olaparib for 48 h. Significant differences were analyzed using the two-sided Student's t-test. Asterisks indicate *p*-values < 0.05. Bars = mean ± SD; *n* = 3 independent experiments (per condition). **B** Annexin assay of SK-UT-1 treated with 0.1% DMSO, 0.5 μM OTS186935, 1 μM olaparib, and 0.5 μM OTS186935 + 1 μM olaparib for 48 h. The proportion of apoptotic cells was calculated as the sum of the Q2 and Q3 values. Significant differences were analyzed using the two-sided Student's t-test. Asterisks indicate *p*-values < 0.05. Bars = mean ± SD; *n* = 3 independent experiments (per condition). **C** Western blotting of SK-LMS-1 and SK-UT-1 treated with 0.1% DMSO, 0.5 μM OTS186935, 1 μM olaparib, and 0.5 μM OTS186935 + 1 μM olaparib for 48 h. SD, standard deviation; DMSO, dimethylsulfoxide

suppressed γH2AX expression (Fig. 4A and Additional File 8: Fig. S6C).

To confirm the suppression of nuclear γH2AX accumulation, we compared cell immunofluorescence staining results between treatment with 0.5 μM doxorubicin alone and in combination with 1 μM OTS186935. The results showed that OTS186935 reduced γH2AX accumulation in the nucleus (Fig. 4B). Additionally, immunofluorescence staining for TP53BP1—a downstream marker of double-strand DNA breaks—revealed decreased expression levels following treatment with OTS186935 (Fig. 4B and Additional file 7: Fig. S5).

ChIP-seq was performed on SK-UT-1 cells to further investigate the effect of OTS186935 on γH2AX distribution. ChIP-seq was conducted under four conditions: 0.1% DMSO (negative control), 1 μM OTS186935, 0.5 μM doxorubicin, and a combination of 1 μM OTS186935 with 0.5 μM doxorubicin. The samples were immunoprecipitated using an anti-γH2AX antibody. The results demonstrated that treatment with OTS186935 reduced the γH2AX signal, indicating decreased genomic accumulation of γH2AX, and that OTS186935 attenuated damage-induced accumulation and double-strand DNA break modulation (Fig. 4C, D).

Effects of the combination of OTS186935 and olaparib in in vivo experiments

Compared to the control group, the OTS186935 and combination groups demonstrated a significant decrease in tumor volume ($p = 0.012$; Fig. 5A and B). The decrease in tumor volume in the combination group was greater than that in the OTS186935 group ($p = 0.59$). No significant loss in body weight was observed during treatment in any of the groups (Fig. 5C), and toxicity was not detected.

Discussion

In this study, *SUV39H2* expression was increased in uLMS, suggesting that it is involved in carcinogenesis and that SUV39H2 inhibitors are a novel therapeutic strategy for uLMS. We also demonstrated the effects of the combination of OTS186935 and olaparib in uLMS cell lines and found that it was effective in a 53BP1-deficient uLMS cell line. OTS186935 alone induced cell cycle arrest, whereas the addition of olaparib induced apoptosis and cell cycle arrest in 53BP1-deficient uLMS cells. OTS186935 also decreased γH2AX accumulation, indicating attenuated damage-induced γH2AX accumulation and double-strand DNA repair modulation.

The prognosis of uLMS is poor, underscoring the need for novel therapeutic strategies. We focused on SUV39H2 because it is related to carcinogenesis in various types of cancers [21–23]. The results of the drug sensitivity assay indicated that OTS186935 showed sensitivity to uLMS cell lines (Fig. 1C). In vivo experiments revealed the efficacy of OTS186935 in uLMS (Fig. 5A and B).

Recently, PARP inhibitors have become increasingly important for treating gynecological tumors with HRD, as 25% of patients with uLMS have HRD [9]. Case reports have used PARP inhibitors for uLMS, and phase II clinical trials of PARP inhibitors for uLMS have begun [7, 8]. Furthermore, the combination of temozolomide and olaparib is currently being investigated in clinical trials [33], based on the rationale that combining PARP inhibitors with other agents may overcome acquired resistance and provide synergistic efficacy. HRR, where BRCA1/2 is mainly involved, and NHEJ, in which 53BP1 is involved, function independently. Therefore, in HRD, 53BP1-based NHEJ can be dominant, whereas when mutations of NHEJ-related factors, such as *53BP1*, *RIF1*, and *REV7*, are present, NHEJ dominance can be lost; this is one of the mechanisms by which HRR is activated even in *BRCA* mutations and how resistance to PARP inhibitors is acquired [10, 34].

Strategies to resolve this resistance to PARP inhibitors are required, and combination therapies are being investigated. Karakashev et al. reported that in high-grade serous ovarian carcinoma with high *CARM1* expression, *EZH2* represses the *MAD2L2* promoter, which promotes NEHJ via histone methylation (H3K27me3). EZH2 inhibition induces NHEJ dominance, resulting in a synthetic lethal mechanism involving PARP inhibitors [18]. Our results demonstrated the synthetic lethality of OTS186935 combined with olaparib in a 53BP1-deficient uLMS cell line. Although in vivo experiments showed no significant difference between the OTS186935 and combination groups, combination therapy tended to be superior to OTS186935 alone. SUV39H2 is associated with DNA damage-induced γH2AX, and SUV39H2 suppression reduces γH2AX accumulation [19]. Notably, in gastric cancer, m^6A-modified SUV39H2 represses DUSP6, enhancing ATM phosphorylation and HRR [35]; when SUV39H1/2 is defective, cells appear to have HRD-like states [20]. Together with evidence

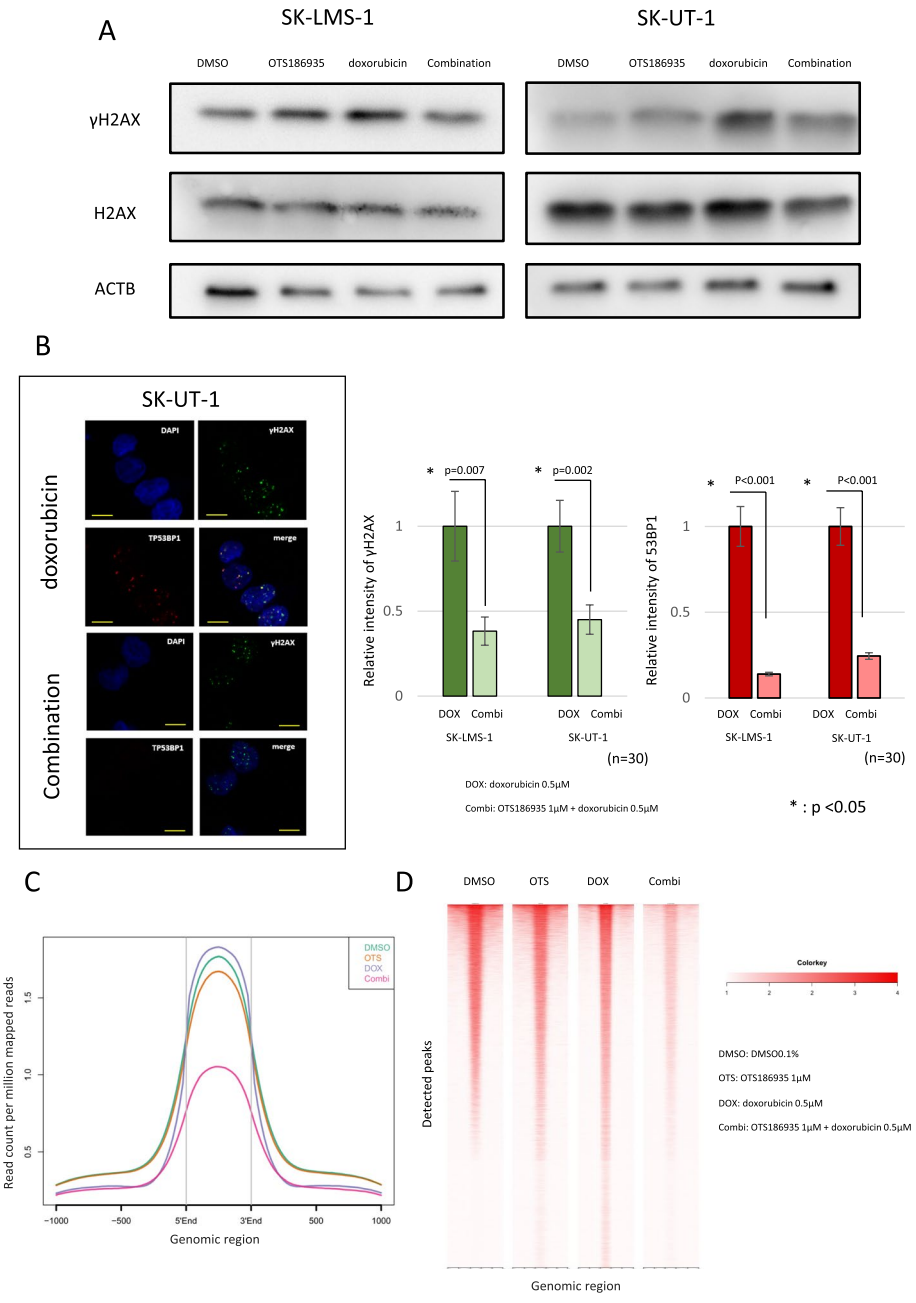

Fig. 4 Mechanism of OTS186935 on the DNA break repair pathway. **A** Western blotting of SK-LMS-1 and SK-UT-1 treated with 0.1% DMSO as a negative control, 1 μM OTS186935, 0.5 μM doxorubicin for DNA damage induction, and 1 μM OTS186935 + 0.5 μM doxorubicin for 1 h. **B** Cell immunofluorescence staining of SK-LMS-1 and SK-UT-1 treated with 0.5 μM doxorubicin only for DNA damage induction and 1 μM OTS186935 + 0.5 μM doxorubicin (Combination) for 1 h. The relative intensity of γH2AX and TP53BP1 in each cell was estimated using the ImageJ software. Significant differences were analyzed using the two-sided Student's t-test. Asterisks indicate *p*-values < 0.05. Bars = mean ± SD; *n* = biological replicates. Yellow bars indicate 10 μm in the images. Representative SK-LMS-1 images are provided in Fig. S5 (Additional file 7). **C** ChIP-seq for SK-UT-1 treated with 0.1% DMSO as a negative control, 1 μM OTS186935, 0.5 μM doxorubicin for DNA damage induction, and 1 μM OTS186935 + 0.5 μM doxorubicin for 1 h. Average γH2AX-ChIP-seq signal in SK-UT-1 cells treated with 0.1% DMSO as a negative control, 1 μM OTS186935, 0.5 μM doxorubicin for DNA damage induction, and 1 μM OTS186935 + 0.5 μM doxorubicin for 1 h. (Peak center ± 1 kb) (**D**) Heatmaps of γH2AX-ChIP-seq in SK-UT-1 cells treated with 0.1% DMSO as a negative control, 1 μM OTS186935, 0.5 μM doxorubicin for DNA damage induction, and 1 μM OTS186935 + 0.5 μM doxorubicin for 1 h. Heatmaps are sorted by γH2AX-ChIP-seq signal in descending order (Peak center ± 1 kb). SD, standard deviation; ChIP-seq, chromatin immunoprecipitation sequencing; γH2AX, phosphorylated H2AX

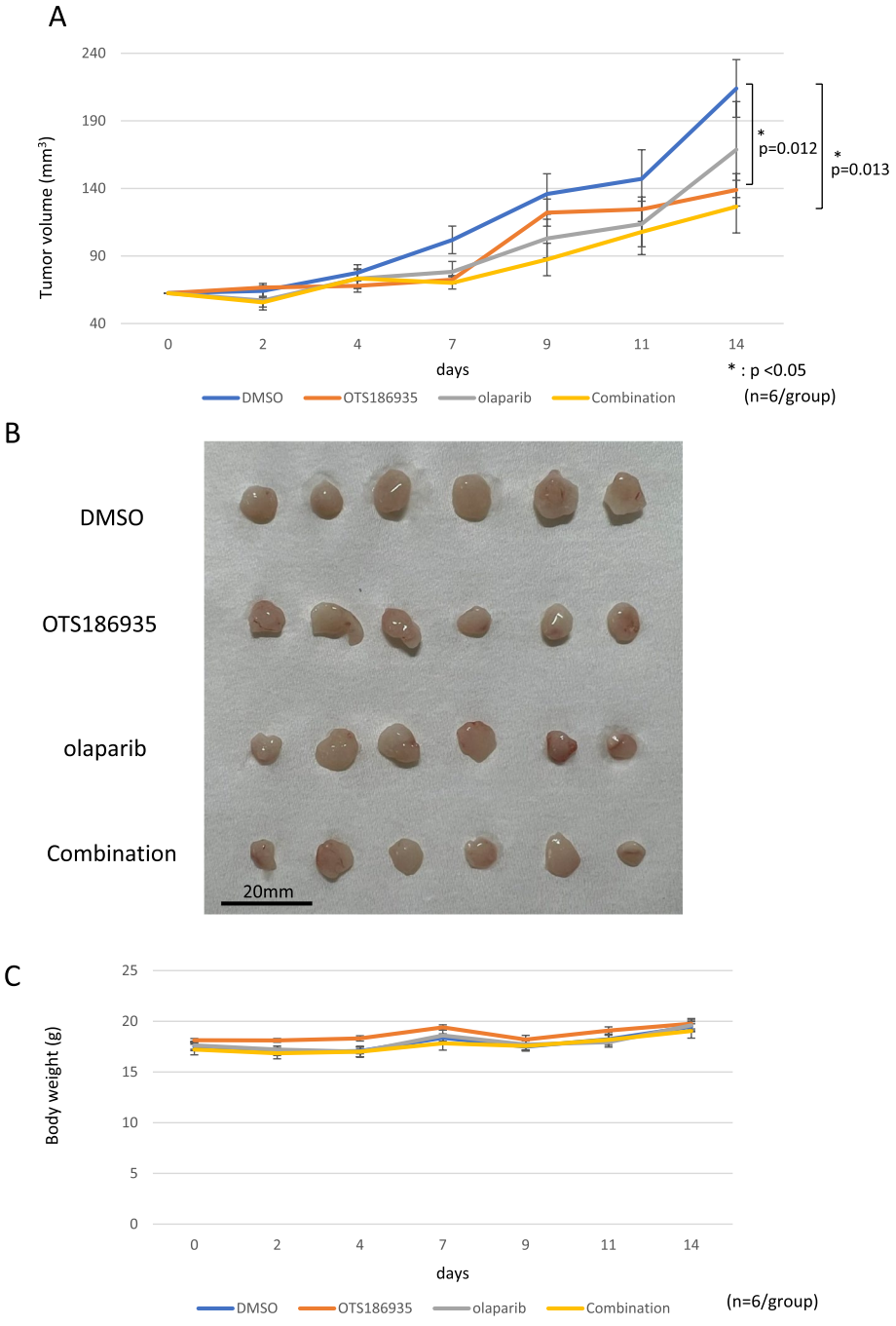

Fig. 5 Effects of OTS186935 + olaparib in vivo (**A)** Mice bearing SK-UT-1 cells ($n = 6$ per group) were intraperitoneally treated once daily with DMSO as the control group, OTS186935 10 mg/kg body weight as the OTS186935 group, olaparib 50 mg/kg as the olaparib group, and OTS186935 10 mg/kg + olaparib 50 mg/kg as the combination group for 14 days. Statistical testing was performed as pairwise two-group comparisons between prespecified pairs (e.g., control vs. OTS186935, control vs. olaparib, OTS186935 vs. olaparib, and combination vs. each monotherapy). Significant differences were analyzed using the two-sided Student's t-test. Asterisks indicate *p*-values < 0.05. Bars = mean ± SD; n = biological replicates. **B** Images of tumors treated as described above. **C** Mean body weight ± SD treated as above. n = biological replicates. SD, standard deviation; DMSO, dimethylsulfoxide

that SUV39H2 facilitates HRR, its inhibition may shift repair toward HRD-like states, potentially explaining increased sensitivity to PARP inhibitors. It is hypothesized that OTS186935 inhibits the double-strand DNA repair mechanism, as represented by the reduced γH2AX accumulation, while olaparib acts as an inhibitor of the single-strand repair mechanism. Furthermore, OTS186935 may exert inhibitory effects on HRR in cell lines in where HRR is activated by the *53BP1* mutation, because SUV39H2 is a key factor in HRR, thereby

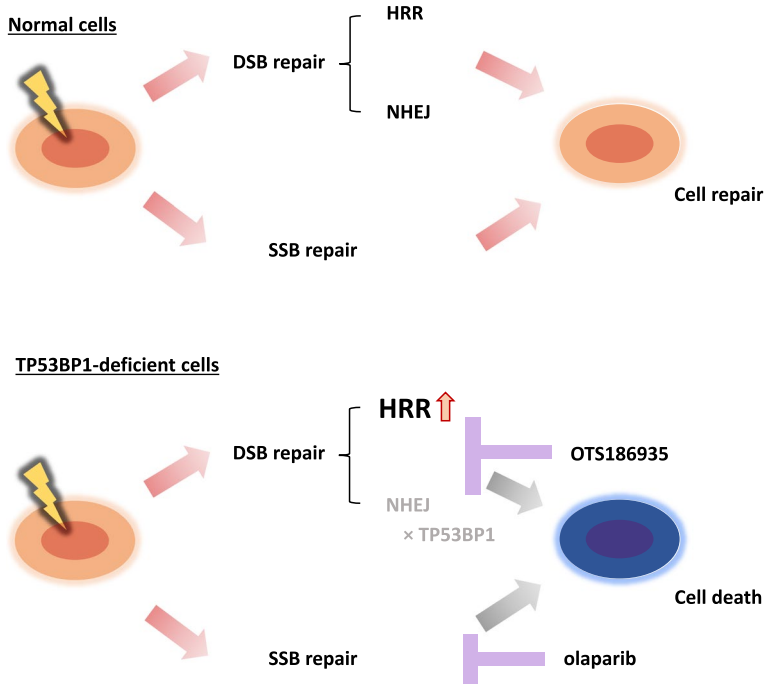

Fig. 6 Hypothesis of mechanisms on the synthetic lethality of OTS186935 and olaparib OTS186935 inhibits the double-strand DNA repair mechanism, as represented by the inhibition of γH2AX accumulation, whereas olaparib acts as an inhibitor of the single-strand repair mechanism. OTS186935 may produce a greater inhibitory effect on double-strand DNA repair in cell lines where HR is activated by the 53BP1 mutation, thereby inducing a synergistic effect. SSB, single-strand break; DSB, double-strand break; HRR, homologous recombination repair; NHEJ, non-homologous end joining

inducing a synergistic effect (Fig. 6). To the best of our knowledge, this is the first study in uLMS to evaluate the preclinical antitumor activity of an SUV39H2 inhibitor and its combination with a PARP inhibitor.

This study had some limitations. Due to the small sample size, the apparent increase in *SUV39H2* did not reach two-sided statistical significance and showed significance only under a prespecified one-sided test, indicating a trend rather than definitive evidence. Validation in larger, independent cohorts is warranted. Additionally, the number of cell lines was limited; experiments were conducted in two uLMS cell lines only, which may restrict generalizability. Although we focused on *53BP1* because of the differences between the two cell lines, other genes may have been involved in this synergistic effect. Therefore, further validation is required to confirm these mechanisms. Furthermore, we observed a decrease in H3K9me3 levels after treatment with OTS186935. However, no relationship was observed between H3K9me3 and synthetic lethality.

Conclusion

OTS186935 showed efficacy in uLMS cell lines in vitro and in vivo. Combination therapy with olaparib resulted in synthetic lethality in 53BP1-deficient cell lines. We inferred that OTS186935 inhibits double-strand DNA break repair by suppressing γH2AX accumulation, thereby inducing synthetic lethality when combined with olaparib.

Abbreviations

uLMS	Uterine leiomyosarcoma
γH2AX	Phosphorylated H2AX
ChIP-seq	Chromatin immunoprecipitation sequencing
PARP	Poly (ADP-ribose) polymerase
HRD	Homologous recombination repair defect
NHEJ	Non-homologous end joining
SUV39H2	Suppressor license of variegation 3–9 homolog 2
H3K9me3	Histone H3 lysine 9
HRR	Homologous recombination repair
IHC	Immunohistochemical staining
E-MEM	Eagle's minimum essential medium
RT-qPCR	Real-time quantitative polymerase chain reaction
PS	Proportion score
IS	Intensity score
DMSO	Dimethylsulfoxide
CI	Combination index
IC50	Half-maximal inhibitory concentration
SDS	Sodium dodecyl sulfate
BSA	Bovine serum albumin
RNA-seq	RNA sequencing

Supplementary Information

The online version contains supplementary material available at https://doi.org/10.1186/s12885-025-15267-6.

Additional file 1. Supplementary tables.

Additional file 2. Fig. S1A. Drug Sensitivity Assays for EPZ-6438.

Additional file 3. Fig. S1B. Images of immunohistochemical staining results for SUV39H2 in clinical samples.

Additional file 4. Fig S2. Cell viability with OTS186935 ± olaparib (2.5 μM) in uLMS cell lines.

Additional file 5. Fig S3. Annexin assay of SK-LMS-1 cells treated with 0.1% DMSO, 0.5 μM OTS186935, 1 μM olaparib, and 0.5 μM OTS186935 + 1 μM olaparib for 48 h.

Additional file 6. Fig. S4(A) The results of RNA-seq of SK-UT-1 cells (B) Immunofluorescence staining of SK-LMS-1 and SK-UT-1 cells.

Additional file 7. Fig. S5. Immunofluorescence staining of SK-LMS-1 cells.

Additional file 8. Fig. S6. The original and medium contrast images of western blotting.

Acknowledgements
The authors are grateful to Dr. Liying Yang (Division of Cancer Epigenomics, Cancer Institute, Japanese Foundation for Cancer Research, Tokyo, Japan) for helping with our sequencing analysis. The authors would like to thank Editage for the English language review.

Authors' contributions
YT: Data curation, investigation, formal analyses, methodology, visualization, writing (original draft), and writing (review and editing). KS: conceptualization, data curation, funding acquisition, methodology, project administration, writing (original draft), and writing (review and editing). KK: Data curation, formal analysis, investigation, and methodology. YY: investigation, methodology, and writing (review and editing). RH: investigation, methodology, and writing (review and editing). AK: Data curation, investigation, methodology, and writing (review and editing). AT: data curation, investigation, methodology, and writing (review and editing); MI: investigation and writing (review and editing). YM: Supervision and writing (review and editing). MT: Methodology, supervision, and writing (review and editing). TI: Supervision and writing (review and editing). MM: Supervision and writing (review and editing). RH: Supervision and writing (review and editing). TU: Supervision and writing (review and editing). KO: Methodology, supervision, and writing (review and editing). YH: supervision and writing (review and editing). RM: conceptualization, methodology, supervision, and writing (review and editing). YO: Supervision and writing (review and editing).

Funding
This study is partially supported by BRIDGE < programs for Bridging the gap between R&d and the IDeal society (society 5.0) and Generating Economic and social value >

Data availability
The RNA sequencing and ChIP sequencing data generated in this study have been deposited in the NCBI Gene Expression Omnibus (GEO) under the accession numbers GSE297689 and GSE297686, respectively. These datasets are publicly available at https://www.ncbi.nlm.nih.gov/geo.

Declarations

Ethics approval and consent to participate
All patients were diagnosed by pathologists (certified as specialists by the Japanese Society of Pathology) at the University of Tokyo Hospital. This study was approved by The Human Genome, Gene Analysis Research Ethics Committee of the University of Tokyo, and written informed consent was obtained from each patient (G0683-(26)). This study was conducted in accordance with the principles of the Declaration of Helsinki.

Consent for publication
Not applicable.

Competing interests
The authors declare no competing interests.

Author details
[1]Department of Obstetrics and Gynecology, Graduate School of Medicine, The University of Tokyo, Tokyo, Japan
[2]Division of Cancer Epigenomics, Cancer Institute, Japanese Foundation for Cancer Research, Tokyo, Japan
[3]Cancer Cell Diversity Project, NEXT-Ganken Program, Japanese Foundation for Cancer Research, Tokyo, Japan
[4]Department of Pathology, Graduate School of Medicine, The University of Tokyo, Tokyo, Japan
[5]Division of Medical AI Research and Development, National Cancer Center Research Institute, Tokyo, Japan
[6]Cancer Translational Research Team, RIKEN Center for Advanced Intelligence Project, Tokyo, Japan
[7]Division of Integrative Genomics, Graduate School of Medicine, The University of Tokyo, Tokyo, Japan

Received: 28 May 2025 / Accepted: 28 October 2025
Published online: 16 December 2025

References

1. Desar IME, Ottevanger PB, Benson C, van der Graaf WTA. Systemic treatment in adult uterine sarcomas. Crit Rev Oncol Hematol. 2018;122:10–20.
2. Muss HB, Bundy B, DiSaia PJ, Homesley HD, Fowler WC Jr, Creasman W, et al. Treatment of recurrent or advanced uterine sarcoma. A randomized trial of doxorubicin versus doxorubicin and cyclophosphamide (a phase III trial of the Gynecologic Oncology Group). Cancer. 1985;55:1648–53.
3. Prat J, Mbatani N. Uterine sarcomas. Int J Gynaecol Obstet. 2015;131:S105-10.
4. van der Graaf WT, Blay JY, Chawla SP, Kim DW, Bui-Nguyen B, Casali PG, et al. Pazopanib for metastatic soft-tissue sarcoma (PALETTE): a randomised, double-blind, placebo-controlled phase 3 trial. Lancet. 2012;379:1879–86.
5. Demetri GD, von Mehren M, Jones RL, Hensley ML, Schuetze SM, Staddon A, et al. Efficacy and safety of trabectedin or dacarbazine for metastatic liposarcoma or leiomyosarcoma after failure of conventional chemotherapy: results of a phase III randomized multicenter clinical trial. J Clin Oncol. 2016;34:786–93.
6. Schöffski P, Chawla S, Maki RG, Italiano A, Gelderblom H, Choy E, et al. Eribulin versus dacarbazine in previously treated patients with advanced liposarcoma or leiomyosarcoma: a randomised, open-label, multicentre, phase 3 trial. Lancet. 2016;387:1629–37.
7. Asano H, Oda K, Yoshihara K, Ito YM, Matsumura N, Shimada M. Phase II study of niraparib in recurrent or persistent rare fraction of gynecologic malignancies with homologous recombination deficiency (JGOG2052). J Gynecol Oncol. 2022;33:e55.
8. Shammas N, Yang T, Abidi A, Amneus M, Hodeib M. Clinical use of PARP inhibitor in recurrent uterine leiomyosarcoma with presence of a somatic BRCA2 mutation. Gynecol Oncol Rep. 2022;42:101044.
9. Choi J, Manzano A, Dong W, Bellone S, Bonazzoli E, Zammataro L, et al. Integrated mutational landscape analysis of uterine leiomyosarcomas. J Proc Natl Acad Sci U S A. 2021;13:118.
10. D'Andrea AD. Mechanisms of PARP inhibitor sensitivity and resistance. DNA Repair. 2018;71:172–6.
11. Cheng Y, He C, Wang M, Ma X, Mo F, Yang S, et al. Targeting epigenetic regulators for cancer therapy: mechanisms and advances in clinical trials. Signal Transduct Target Ther. 2019;4:62.
12. de Almeida BC, Dos Anjos LG, Dobroff AS, Baracat EC, Yang Q, Al-Hendy A, et al. Epigenetic features in uterine leiomyosarcoma and endometrial stromal sarcomas: an overview of the literature. Biomedicines. 2022;10:2567.
13. Straining R, Eighmy W. Tazemetostat: EZH2 inhibitor. J Adv Pract Oncol. 2022;13:158–63.
14. Inoue F, Sone K, Toyohara Y, Tanimoto S, Takahashi Y, Kusakabe M, et al. Histone arginine methyltransferase CARM1 selective inhibitor TP-064 induces apoptosis in endometrial cancer. Biochem Biophys Res Commun. 2022;601:123–8.
15. Inoue F, Sone K, Kumegawa K, Hachijo R, Suzuki E, Tanimoto S, et al. Inhibition of protein arginine methyltransferase 6 activates interferon signaling and induces the apoptosis of endometrial cancer cells via histone modification. Int J Oncol. 2024;64:32.
16. Kukita A, Sone K, Kaneko S, Kawakami E, Oki S, Kojima M, et al. The histone methyltransferase SETD8 regulates the expression of tumor suppressor genes via H4K20 methylation and the p53 signaling pathway in endometrial cancer cells. Cancers (Basel). 2022;14:5367.
17. Kukita A, Sone K, Oda K, Hamamoto R, Kaneko S, Komatsu M, et al. Histone methyltransferase SMYD2 selective inhibitor LLY-507 in combination with

poly ADP ribose polymerase inhibitor has therapeutic potential against high-grade serous ovarian carcinomas. Biochem Biophys Res Commun. 2019;513:340–6.
18. Karakashev S, Fukumoto T, Zhao B, Lin J, Wu S, Fatkhutdinov N, et al. EZH2 inhibition sensitizes CARM1-high, homologous recombination proficient ovarian cancers to PARP inhibition. Cancer Cell. 2020;37:157-67.e6.
19. Sone K, Piao L, Nakakido M, Ueda K, Jenuwein T, Nakamura Y, et al. Critical role of lysine 134 methylation on histone H2AX for γ-H2AX production and DNA repair. Nat Commun. 2014;5(1):5691.
20. Alagoz M, Katsuki Y, Ogiwara H, Ogi T, Shibata A, Kakarougkas A, et al. SETDB1, HP1 and SUV39 promote repositioning of 53BP1 to extend resection during homologous recombination in G2 cells. Nucleic Acids Res. 2015;43:7931–44.
21. Zheng Y, Li B, Wang J, Xiong Y, Wang K, Qi Y, et al. Identification of SUV39H2 as a potential oncogene in lung adenocarcinoma. Clin Epigenetics. 2018;10:129.
22. Chao C, You J, Li H, Xue H, Tan X. Elevated SUV39H2 attributes to the progression of nasopharyngeal carcinoma via regulation of NRIP1. Biochem Biophys Res Commun. 2019;510:290–5.
23. Vougiouklakis T, Saloura V, Park JH, Takamatsu N, Miyamoto T, Nakamura Y, et al. Development of novel SUV39H2 inhibitors that exhibit growth suppressive effects in mouse xenograft models and regulate the phosphorylation of H2AX. Oncotarget. 2018;9:31820–31.
24. Chou TC. Theoretical basis, experimental design, and computerized simulation of synergism and antagonism in drug combination studies. Pharmacol Rev. 2006;58:621–81.
25. Jiang H, Lei R, Ding SW, Zhu S. Skewer: a fast and accurate adapter trimmer for next-generation sequencing paired-end reads. BMC Bioinformatics. 2014;15:182.
26. Dobin A, Davis CA, Schlesinger F, Drenkow J, Zaleski C, Jha S, et al. STAR: ultrafast universal RNA-seq aligner. Bioinformatics. 2013;29:15–21.
27. Liao Y, Smyth GK, Shi W. Featurecounts: an efficient general purpose program for assigning sequence reads to genomic features. Bioinformatics. 2014;30:923–30.
28. Robinson JT, Thorvaldsdóttir H, Wenger AM, Zehir A, Mesirov JP. Variant review with the integrative genomics viewer (IGV). Cancer Res. 2017;77:e31-4.
29. Langmead B, Salzberg SL. Fast gapped-read alignment with Bowtie 2. Nat Methods. 2012;9:357–9.
30. Quinlan AR, Hall IM. BEDtools: a flexible suite of utilities for comparing genomic features. Bioinformatics. 2010;26:841–2.
31. Zhang Y, Liu T, Meyer CA, Eeckhoute J, Johnson DS, Bernstein BE, et al. Model-based analysis of ChIP-Seq (MACS). Genome Biol. 2008;9:R137.
32. Shen L, Shao N, Liu X, Nestler E. ngs.plot: quick mining and visualization of next-generation sequencing data by integrating genomic databases. BMC Genomics. 2014;15:284.
33. Ingham M, Allred JB, Chen L, Das B, Kochupurakkal B, Gano K, et al. Phase II study of olaparib and temozolomide for advanced uterine leiomyosarcoma (NCI protocol 10250). J Clin Oncol. 2023;41:4154–63.
34. Zou Y, Zhang H, Chen P, Tang J, Yang S, Nicot C, et al. Clinical approaches to overcome PARP inhibitor resistance. Mol Cancer. 2025;24:156.
35. Yang J, Xu P, Chen Z, Zhang X, Xia Y, Fang L, et al. N6-methyadenosine modified SUV39H2 regulates homologous recombination through epigenetic repression of DUSP6 in gastric cancer. Cancer Lett. 2023;558:216092.

Publisher's Note